ICSV13 - Vienna
The Thirteenth International Congress on Sound and Vibration
Vienna, Austria, July 2-6, 2006

Advanced Features in Computational Acoustics

R. Lerch and M. Kaltenbacher

Department of Sensor Technology, Friedrich-Alexander-University Erlangen-Nuremberg
Paul-Gordan-Strasse 3/5, D-91052 Erlangen, Germany

Abstract
In this paper we will address some important technical features of finite element (FE) codes used in computational acoustics. We will present schemes (i) to determine discretization errors, (ii) to handle frequency dependent damping along the propagation paths of acoustic waves, (iii) perfectly matched layers for the efficient treatment of open domain problems in the frequency domain, and (iv) to combine FE-meshes (subdomains) with quite different mesh sizes at the boundary of the subdomains, so called non-matching grids.

INTRODUCTION

Modern numerical simulation tools allow a precise analysis of the generation and propagation of sound. However, up to now, a variety of computational features enhancing their applicability are missing in these codes. Therefore, it is sometimes cumbersome to come to practically useful results when applying such numerical codes to real life problems. In this paper, some of these lacking features will be addressed and, furthermore, their implementation and test in a finite element environment is reported.
When computing the propagation of sound over long distances the numerical errors due to spatial and time **discretization errors** will accumulate. Many sound propagation media exhibit **frequency dependent damping**. This asks for special treatment within finite element codes. We will demonstrate how damping with an arbitrary frequency dependent damping coefficient can be handled by finite elements for time domain analysis. When using finite elements in open domain problems one has to overcome the difficulty of reflexions at the boundaries of the computational domain. We will present a new technique based on **Perfectly Matched Layers (PML)**. When computing sound in neighbouring domains with quite different propagation velocities (wavelengths) it is useful to use different finite element grids for these domains. We present a scheme for which it is not necessary that the grids match at their neighbouring boundaries. These are called **non-matching grids**.

DISCRETIZATION ERROR

It is a well known phenomena, that the application of the classical Galerkin-FEM leads to an increasing numerical error with increasing acoustic wave number $k = \omega/c = 2\pi f/c$ (f and c denotes the frequency and speed of sound). The main effect is due to numerical dispersion, which shows a numerical wave number k^h being different from the continuous wave number k. Therewith, the acoustic waves propagate with a wrong sound speed and show a phase shift compared to the analytical solution.
The numerical error can be derived as a function of the wave number k and the discretization parameter h [8]

$$e_h \leq C_1\theta + C_2 k\,\theta^2 \quad \text{with } \theta = kh \tag{1}$$

$$e_h = \frac{|p' - p'_h|_1}{|p'|_1} \quad \text{with } |u|_1 = \sqrt{\int \left(\frac{\partial u}{\partial x}\right)^2 dx}\,. \tag{2}$$

In (1) - (2) C_1, C_2 denote constants which are independent of θ. The first term in (1) describes the approximation error, which can be effectively controlled by using accordingly smaller mesh sizes h by increasing wave number k. However, the second term in (1) denotes the *pollution-error*, which increases with k^3 and which leads to severe problems for large wave numbers. In [1] a general formula for this error including the order of the finite element shape functions (p-FEM) can be found, and it is shown, that this part of the error can just be effectively controlled by increasing order of the finite element shape functions.

FREQUENCY DEPENDENT DAMPING OF PROPAGATION MEDIUM

The damping of acoustic waves along their propagation paths is an imprortant issue which has to be addressed within precise computer simulations of acoustic phenomena. Damping in the megahertz range for biological matter, for example, suggest the description with a frequency dependency according to a power law. With the two material parameters α_0 and y we can make the following ansatz for the damping coefficient α

$$\alpha(\omega) = \alpha_0 |\omega|^y\,, \quad 0 < y \leq 2\,. \tag{3}$$

For most soft tissue we find that the frequency power factor y lies between 1.0 and 1.5. For $y \neq 2$ phase dispersion is observed to occur. The power factor is a material characteristics and an accurate determination is one of the goals of according measurements [2]. Because the diffraction error is frequency dependent, the shape of retrieved damping and dispersion curves is altered, hence falsified values of y are determined. Popular corrections of diffraction effects use approximative solutions to the analytical approach already discussed in [2]. Admittedly, those corrections neglect damping in the propagation path and are only valid for plane faced transducers. In our approach we retrieve such correction of diffraction from finite element simulations.

Because we are solely utilizing axisymmetric transmitters and receivers, we are able to perform the simulations in a 2D axisymmetric setup. In the simulations described in the following we chose the distance between transducer and receiver to be $z = 10\ cm$, which is owed to the size of the mesh of 2.35 million quadrilateral finite elements.
We incorporated attenuation with a power law frequency dependency and dispersion calculated from Kramers-Kronig relations. Both can be combined to a single term in the time domain wave equation [11], which was implemented for transient simulations using a fractional derivative. In theory the computation of fractional derivatives requires the whole history of the function in a weighted form. For a time discrete function of the acoustic pressure p'_{n+1} at time step $n+1$ the fractional derivative of order y can be expressed as

$$D^y p'_{n+1} = \sum_{k=0}^{n+1} w_k \cdot p'_{n+1-k} \ , \tag{4}$$

where D^y denotes the fractional derivative operator. In contrast, derivatives of integer order depend solely on the local behavior. Beforehand, two popular algorithms for computing (4) were evaluated. The first algorithm is based on generalized finite differences and is mostly referred to by the names of Grünwald and Letnikov in literature (see e.g. Gorenflo [7] for a description). Luise Blank published a collocation approximation with polynomial splines [6], which we used as second algorithm. With the latter algorithm, we were able to achieve a relative error of less than 0.1 % after 10 cm of propagation (corresponds to seventy wavelengths).
For demonstration, we investigated a bone sample of thickness $d = 1\ cm$ with a propagation velocity of $c_s = 3200\frac{m}{s}$. Now, the frequency dependent damping of bone with parameters $\alpha_0 = 1.6633 \cdot 10^{-6}$ and frequency power factor $y = 1.1$ is taken into account. For water we use thermoviscous damping with the values $\alpha_0 = 6.1 \cdot 10^{-16}$ and $y = 2$.
In Fig. 1 the analytical solution (analyt.) is compared with the solutions retrieved from two FE-simulations, where thermoviscous damping ($\alpha \propto \omega^2$) and fractional damping ($\alpha \propto \omega^y$) was applied to the sample region. In the thermoviscous case, the parameter α_0 was adapted so that the value of the damping coefficient α equals the one of the fractional damping model for a frequency of 1 MHz. Absolute value and phase of the correction function utilizing thermoviscous damping stay close to the analytical solution, which can be explained with the similar frequency dependence of damping in the sample and reference simulation. For the fractional damping model the curves differ greatly. We conclude from this that the frequency dependence of damping has an influence on the shape of the correction function, so for accurate results the correct damping behavior has to be considered.

PERFECTLY MATCHED LAYERS

One of the great challenges for each volume discretization scheme is the precise modeling of free radiation problems. The crucial point for these computations is, that the numerical scheme avoids any reflections at the computational boundaries. To achieve this requirement, we have

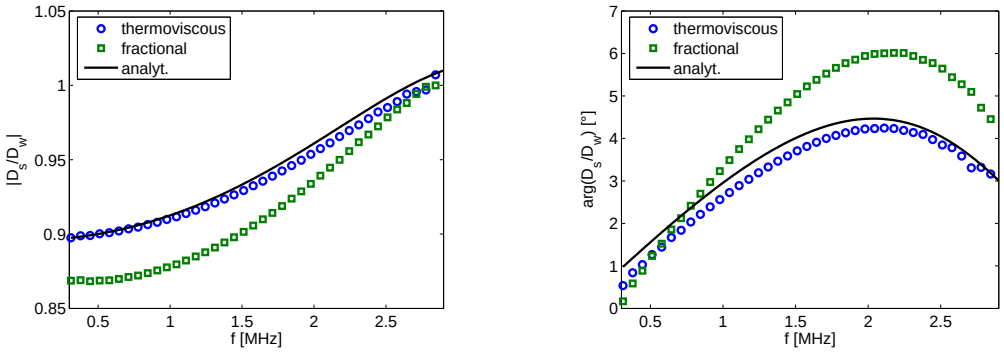

Figure 1: Comparison of the thermoviscous and fractional damping model for bone material. D_s and D_w represent the complex diffraction correction functions for the sample (D_s) and water (D_w).

developed an enhanced PML (Perfectly Matched Layer) method, which allows computational domains being a fraction of the acoustic wavelength.
We start at the mass as well as momentum conservation equations for linear acoustics, which read as follows

$$\frac{\partial p'}{\partial t} = -\rho_0 c^2 \boldsymbol{\nabla} \mathbf{v}' \tag{5}$$

$$\frac{\partial \mathbf{v}'}{\partial t} = -\frac{1}{\rho_0} \boldsymbol{\nabla} p' \,. \tag{6}$$

In (5) and (6) p' denotes the acoustic pressure, $\mathbf{v}'$ the particle velocity, ρ_0 the mean density of the fluid and c the speed of sound. According to [4] we apply a splitting of the acoustic pressure p' into p'_x, p'_y and p'_z. Therewith, the mass as well as momentum conservation equation for linear acoustics change to

$$\frac{\partial p'_x}{\partial t} + \sigma_x p'_x = -\rho_0 c^2 \frac{v'_x}{\partial x} \quad \frac{\partial v'_x}{\partial t} + \sigma_x v'_x = -\frac{1}{\rho_0} \frac{\partial p'}{\partial x} \tag{7}$$

$$\frac{\partial p'_y}{\partial t} + \sigma_y p'_y = -\rho_0 c^2 \frac{v'_y}{\partial y} \quad \frac{\partial v'_y}{\partial t} + \sigma_y v'_y = -\frac{1}{\rho_0} \frac{\partial p'}{\partial y} \tag{8}$$

$$\frac{\partial p'_z}{\partial t} + \sigma_z p'_z = -\rho_0 c^2 \frac{v'_z}{\partial z} \quad \frac{\partial v'_z}{\partial t} + \sigma_z v'_z = -\frac{1}{\rho_0} \frac{\partial p'}{\partial z}. \tag{9}$$

In the above equations σ_x, σ_y and σ_z are damping functions, which are zero within the acoustic propagation domain and which are different from zero within the PML-layer enclosing the acoustic propagation domain. We will investigate damping functions, which are constant all over the PML-layer, which increase quadratically as well as inverse with the distance.
Applying a Fourier-transformation to (7) - (9), we arrive at the following Helmholtz equation

$$\gamma(x_2)\gamma(x_3)\frac{\partial}{\partial x_1}\left(\frac{1}{\gamma(x_1)}\frac{\partial \hat{p}}{\partial x_1}\right) \tag{10}$$

$$+\gamma(x_1)\gamma(x_3)\frac{\partial}{\partial x_2}\left(\frac{1}{\gamma(x_2)}\frac{\partial \hat{p}}{\partial x_2}\right) \tag{11}$$

$$+\gamma(x_1)\gamma(x_2)\frac{\partial}{\partial x_3}\left(\frac{1}{\gamma(x_3)}\frac{\partial \hat{p}}{\partial x_3}\right) \;=\; \gamma(x_1)\gamma(x_2)\gamma(x_3)\,k^2\,\hat{p}\,. \tag{12}$$

with k the acoustic wave number.
In order to evaluate the PML-method, we perform a computation of a 2D example, as displayed in Fig. 2. This example, where we apply an acoustic load at the center, has an analytic

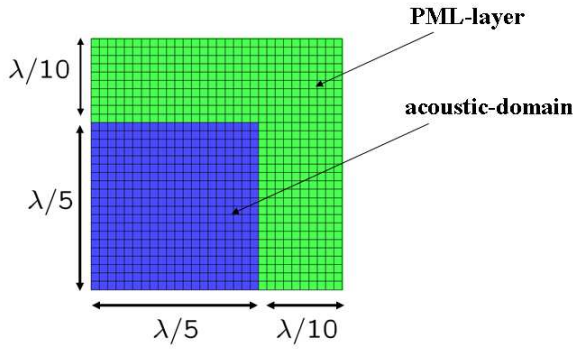

Figure 2: Setup of computational domain

solution according to the Hankel function. Table 1 contains the total L_2-error as well as the relative error at the corner of the propagation region. In Fig. 3 we show the contour lines of the

Table 1: Error evaluation for different damping functions σ

	PML const.	PML quadDist	PML inverseDist
L2-error	0.001613	0.001351	0.001193
rel. Error (λ/5,λ/5)	0.22%	0.135%	0.11%

acoustic pressure inside the propagation as well as PML-region and in Fig. 4 we display the relative error as a contour plot. It has to be noticed, that the Hankel function has a singularity at $(0, 0)$ and, therefore, the comparison between analytical and numerical solution makes no sense near this point.

NON-MATCHING GRIDS

In this section, we face a common problem within computational acoustics, namely that the computational grid in one subdomain can be considerably coarser than in the another subdomain. In order to keep as much flexibility as possible, we use independently generated grids which are well suited for approximating the solution of decoupled local subproblems in each

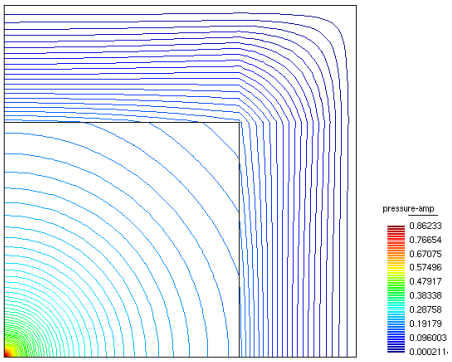

Figure 3: Contour lines of acoustic pressure inside propagation region and PML-region

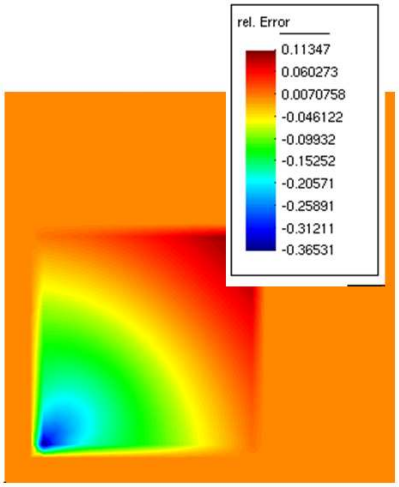

Figure 4: Contour plot of the relative error

subdomain. Therefore, we have to deal with the situation of nonconforming grids appearing at the common interface of two subdomains. Special care has to be taken in order to define and implement the appropriate discrete coupling operators which is published with more detail in [10]. Here, we will briefly deal with the interface condition of the acoustic-acoustic interface and then show results.

For this type of coupled problem, we can use the well-tested and well-studied framework of mortar methods [5]. Both subdomains Ω_1 and Ω_2 are occupied by an acoustic fluid. Thus, in each subdomain we have to solve the wave equation for the acoustic pressures $p_i' : \Omega_i \times (0,T) \to \mathbb{R}$,

$$\frac{1}{c^2}\,\ddot{p}_i' - \Delta\, p_i' = f_i, \quad \text{in} \;\; \Omega_i \times (0,T),\; i = 1,2 \tag{13}$$

completed by appropriate initial conditions at time $t = 0$ and boundary conditions on the global boundary Γ.

For simplicity, we use the same equation and primal variable in both subdomains, and the interface is just artificial, i.e., no material change occurs. We refer to [3, 9] for the treatment of more general situations. Therefore, in the strong setting, it is natural to impose continuity in the trace and flux of the acoustic pressure, along the common interface Γ_{I}, i.e.,

$$p_1' = p_2' \text{ and } \frac{\partial p_1'}{\partial \mathbf{n}} = \frac{\partial p_2'}{\partial \mathbf{n}} \text{ on } \Gamma_{\mathrm{I}}.$$

The flux coupling condition will be enforced in a strong sense by introducing the Lagrange multiplier

$$\lambda = -\frac{\partial p_1'}{\partial \mathbf{n}} = -\frac{\partial p_2'}{\partial \mathbf{n}}, \tag{14}$$

whereas the continuity in the trace will be understood in a weak sense as

$$\int_{\Gamma_{\mathrm{I}}} (p_1' - p_2')\mu \; \mathrm{d}\Gamma = 0, \tag{15}$$

for all test functions μ out of a suitable Lagrange multiplier space. We note that a correct functional framework is presented in [3].
As test example, we choose the domain $\Omega = (-0.05, 0.05)\,\mathrm{m}^2$ and decompose it into $\Omega_1 = (-0.0125, 0.0125)\,\mathrm{m}^2$ and $\Omega_2 = \Omega \setminus \overline{\Omega_1}$. A point source is located at $(0, 0)$ and realized as a Dirichlet node dictating the solution to be

$$u(0, 0, t) = \sin(2\pi f t),$$

with a frequency $f = 1000\,\mathrm{Hz}$. As medium, we choose air, i.e., $c = 343\mathrm{m/s}$. We use a time step size $\Delta t = 10\mu\mathrm{s}$. Figure 5 shows the initial grid and two zooms towards the interface

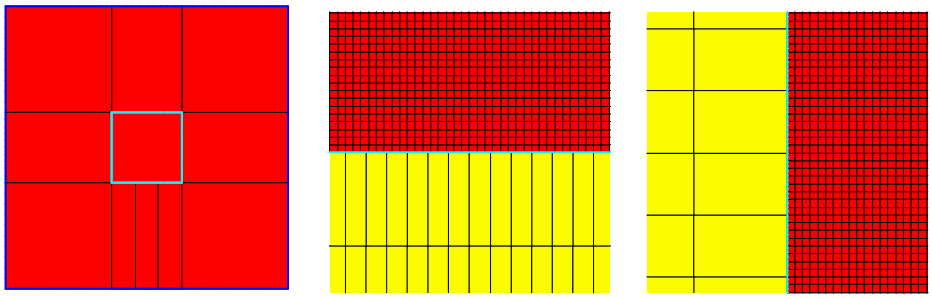

Figure 5: Initial grid, two zooms into the computational grid.

of the actual computational grid, which was obtained by uniformly refining the grid on Ω_1 six times and the one on Ω_2 three times. Thus, on the lower interface side, we have a completely nonconforming situation, whereas on the other sides, the inner interface grid is a pure refinement of the outer one, with a mesh size ratio $h_1/h_2 = 1/8$. In Fig. 6, the isolines of the solutions for two settings after 28 time steps at $t = 280\mu\mathrm{s}$ are plotted. For the left plot,

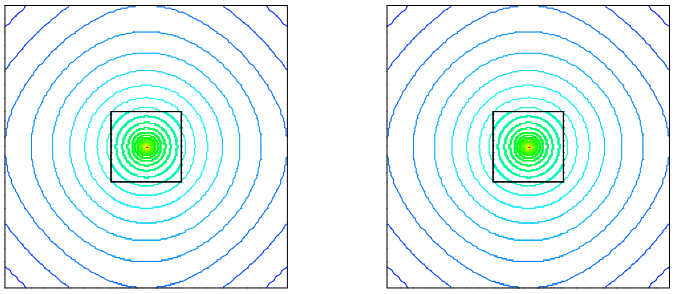

Figure 6: Acoustic pressure contour lines at time $t = 280\mu\mathrm{s}$, Lagrange multipliers defined with respect to the fine side (left) and to the coarse side (right).

the discrete Lagrange multiplier space was chosen with respect to the fine grid on Ω_1, for the right one, it is defined on the coarse grid of Ω_2. There is no qualitative and no noteworthy quantitative difference between both solutions. Thus, for this example, the choice of the grid for the Lagrange multiplier space does not influence the numerical solution. More important,

both solutions are well behaved near the interface and no artificial reflections occur despite the very large difference in the mesh sizes h_1 and h_2.

CONCLUSIONS

In this paper we first addressed some problems within computational acoustics when doing finite element calculations. These are frequency dependent discretization errors as well as damping of the propagation medium. Futhreon, we presented two schemes, which are perfectly matched layers and non-matching grids. When performing calculations in the frequency domain, perfectly matched layers allow the ideal absorption of acoustic energy at the border of the computational domain. Therewith, they are useful for the treatment of open domain problems. Non-matching grids enhance the efficieny and accuracy of finite element calculations which ask for different mesh sizing in different subdomains.

References

[1] M. Ainsworth, SIAM J. Numer. Anal., 42:553–575, 2004

[2] L. Bahr, M. Kaltenbacher, R. Lerch, Proceedings of the IEEE Ultrasonics Symposium, pp. 1687-1690, 2005

[3] A. Bamberger and R. Glowinski and Q. H. Tran, SIAM J. Numer. Anal., 34(2):603–639, 1997

[4] J. P. Berenger, J. Comp. Phys., 114:185–200, 1994

[5] C. Bernardi and Y. Maday and A. T. Patera, in Nonlinear partial differential equations and their applications. Collège de France Seminar, Vol. XI (Paris, 1989–1991), Pitman Res. Notes Math. Ser., 299:13–51, 1994

[6] L. Blank, Nonlinear World, 4:473–490, 1997

[7] R. Gorenflo, in A. Carpinteri and F. Mainardi (editors): Fractals and Fractional Calculus in Continuum Mechanics. Springer Verlag, pp. 277-290, 1997

[8] F. Ihlenburg and I. Babuska, SIAM J. Numer. Anal., 34:315–358, 1997

[9] D. J. P. Lahaye and F. Maggio and A. Quarteroni, East-West J. Numer. Math., 5(4):265–289, 1997

[10] B. Flemisch and M. Kaltenbacher and B. I. Wohlmuth, Int. J. Numer. Meth. Engng, 2006, (in press)

[11] K. R. Waters, M. S. Hughes, G. H. Brandenburger and J. G. Miller, J. A. S. A., 108(5):2114–2119, November 2000. Pt. 1.